Hindawi
Mathematical Problems in Engineering
Volume 2022, Article ID 1038139, 14 pages
https://doi.org/10.1155/2022/1038139

Research Article

Mechanism and Safety Mining Technology of Overall Instability-Induced Rockbursts of Multi-Coal Seam Spatially Isolated Working Face

Bo Sun, Sitao Zhu, Fuxing Jiang, and Gao'ang Wang

School of Civil and Resources Engineering, University of Science and Technology Beijing, Beijing 100083, China

Correspondence should be addressed to Sitao Zhu; zhusitao@ustb.edu.cn

Received 4 August 2022; Accepted 8 September 2022; Published 24 September 2022

Academic Editor: Fuqiang Ren

The isolated working face has always been the hardest hit area for the occurrence of rockburst, and the spatially isolated working face with multiple coal seams is often easily overlooked due to its hidden nature, which leads to the occurrence of rockburst accidents. This paper takes the Liuhuanggou coal mine (9–15) 08 isolated working face as the engineering background, used field research, theoretical analysis, numerical simulation, and field monitoring, investigated the coal body stress evolution law during mining, and revealed the overall instability rockburst mechanism of the working face and deduced the limit advance distance when the working face was in a state of boundary instability. The research results show the following: (1) with the increase of advancement, the overlying strata on the working face are dynamically transformed from the "*C*" spatial structure with hollowing on both sides to the "*θ*" spatial structure with coal body support in the middle; (2) when the dynamic load stress on the coal body of the working face exceeds 1.5 times its integrated compressive strength, there is a risk of overall instability rockburst; (3) when the working face advances to 430 m from the open cutting, the superimposed stress on the coal body exceeds its comprehensive compressive strength and reaches a critical instability state, which is verified by numerical simulation. Based on the analysis of the mechanics and mechanism of the overall instability rockburst of the working face, this paper proposes a set of targeted safe mining solutions: (1) The joint monitoring system of microseism-stress-drilling cutting is adopted to monitor and warn the dangerous rockburst areas. (2) The "rockburst-gas" drilling technique is used to unload the pressure on both sides of the working face and the coal wall. (3) The mining speed shall not exceed 3.2 m/d when the working face is mined before 350 m, and shall not exceed 2.4 m/d when the working face enters the influence area of mined-out LW(4-5)02 (350~550 m). The microseismic monitoring results and field practice confirmed the reasonableness and effectiveness of the safe mining technology plan.

1. Introduction

With the continuous mining of coal resources, the coal deposit conditions are becoming more and more complex, so that rockburst accidents occur frequently [1–8]. According to statistics, the number of rockburst mines in China has rapidly increased from 142 in 2012 to 177 as of 2017, and rockburst has become one of the most dangerous disasters in China's coal mines [9–13]. The frequent occurrence of rockburst has brought serious damage to the safety production and economic efficiency of mines. Among them, the isolated working face, which is generated by strip mining or unreasonable mining layout, is the hardest hit area for the occurrence of rockburst. Compared with other types of working face, the stress concentration around the roadway of an isolated working face is higher, and the roof movement is also more intense. Coupled with the mining conditions, complex geological conditions, and other factors, it is more likely to occur rockburst, which brings great difficulties to the safe mining of coal resources [14–20].

There has been a lot of research on the mechanism and prevention of rockburst induced by the overall instability of the isolated working face. Zhu et al. [21, 22] scientifically classified the types of rockbursts in longwall workings by means of stress and microseismic monitoring, studied the mechanism of overall instability-induced rockbursts, and

proposed a risk assessment method for such rockbursts. Wang et al. [23] and Deng and Gu [24] analyzed the mechanism of mine seismic and rockburst triggered by isolated coal pillars using mechanical models, studied the overlying strata movement law of isolated coal pillars, and proposed reasonable width design criteria for isolated coal pillars. Liu et al. [25] explored the distribution of stress field on the isolated longwall working face by mechanical model, theoretical calculations, seismic computed tomography, and energy density, studied the stress distribution characteristics on the isolated longwall working face under three different surrounding rock conditions, and evaluated the rockburst risk of four longwall isolated working faces in ZhaoLou coal mine as an example. Xue et al. [26] revealed the mechanism of rockburst occurring in mine coal pillars from the perspective of energy evolution and the bursting liability of coal specimen through theoretical calculations and numerical simulations, proposed the energy density criteria for rockburst hazard evaluation, and analyzed the energy density factor and the characteristics of the changing trend in the vertical direction. Zhao et al. [27] established a microstructure model of coal based on the theory of coal grain friction generating charge, studied four different friction coefficient variation laws of coal, and then used the electromagnetic radiation method for potential rockburst ground pressure hazard at isolated coal pillar working face.

The above scholars have conducted a lot of researches on the law of overburden movement of isolated working face and the prevention and control technology of rockburst of isolated working face, which provide theoretical reference for this paper, but there are fewer researches on the critical judgment basis of the overall instability rockburst of coal body and its safe mining technology when the isolated working face with multi-seam spatial distribution advances to the mined-out area. In view of this, this paper takes the Liuhuanggou coal mine (9–15) 08 isolated working face as the engineering background and studies the critical instability width of the isolated working face through mechanical analysis, theoretical calculation, and numerical simulation, in order to provide a reference for similar engineering practice.

2. Engineering Background

2.1. Overview. (9–15) 08 spatially isolated working face(SIW) of the Liuhuanggou coal mine mainly mining 9–15 coal seam. The average mining depth of the working face is 430 m, and the average thickness of the coal seam is 14 m, which belongs to an extra-thick coal seam with stable seams and a simple structure. The roof of the coal seam is dominated by gritstone and medium-grained sandstone, and there is a group of hard sandstone group with a thickness of 26.84 m about 38 m above the coal seam, which may have a large impact on the working face during mining, as shown in Table 1. According to the results of coal rockburst tendency identification, both the 9–15 coal seam and its top and bottom plates have a strong burst tendency.

(9–15) 08 spatially isolated working face(SIW) of the Liuhuanggou coal mine is the successor of (4-5) 06 longwall working face (LW) SIW(9–15) 08 is partially located below the mined-out LW(4-5) 04 and (4-5) 06 of the 4-5 coal seam, and the average distance from 4-5 coal seam is about 27 m. In addition, about 110 m to the southwest of the SIW(9–15) 08 is the old mined-out area of the adjacent mine, and about 548 m to the east from the open cut is the mined-out LW(4-5) 02. It has a strike length of about 1713.2 m and an inclined length of about 130 m. The plan location is shown in Figure 1. The tendency profile is shown in Figures 2 and 3.

Table 1: Stratigraphy statistics table.

Serial number	Lithology	Thickness (m)
R_{19}	Siltstone	1.00
R_{18}	Gritstone	12.80
R_{17}	Interbedded fine-sandstone	5.00
R_{16}	Siltstone	8.04
R_{15}	Mudstone	0.20
R_{14}	Fine-sandstone	3.31
R_{13}	Mudstone	3.42
R_{12}	Fine-sandstone	1.00
R_{11}	Mudstone	2.2
R_{10}	4-5 coal seam	6.94

2.2. Rockburst Risk Analysis. SIW(9–15) 08 has a relatively high degree of stress concentration in the coal body of the working face due to the influence of the extra-thick coal seam, mountain stress, and the mined-out areas on both sides. When the working face advances to mined-out LW(4-5) 02, it gradually forms a spatially isolated working face with four sides of mining, the stress concentration of the coal body on the working face further rises, and the overall instability of the coal body is very likely to occur when mining the coal body in this area, so the coal wall and the trackgate have strong rockburst hazard. The beltgate has a weak rockburst hazard because it is arranged below the mined-out area. In summary, through macro evaluation, the preliminary judgment of (9–15) 08 working face rockburst hazards is shown in Figure 4. This paper focuses on the stress changes in the coal body when the SIW(9–15) 08 is advancing towards the mined-out LW(4-5) 02 and provides safe mining technology solutions based on this, with a view to providing a reference for the actual project.

3. Mechanism of Overall Instability Rockburst

3.1. Overburden Spatial Structure and Stress Evolution Characteristics. According to the actual mining situation of the coal seam in the Liuhuanggou coal mine and the actual measured data of surface subsidence, it is known that during the mining period of SIW(9–15) 08, all the mined-out areas after the mining of 4-5 coal seams are in a non-fully mined state, and the overlying strata of SIW(9–15) 08 form an asymmetric pressure arch structure [28, 29]. With the increasing advancement of the working face, the stress distribution on the coal body roughly shows 4 patterns, as shown in Figure 5.

At the early stage of mining, the coal body of SIW(9–15) 08 is affected by the mined-out areas which on both sides, the

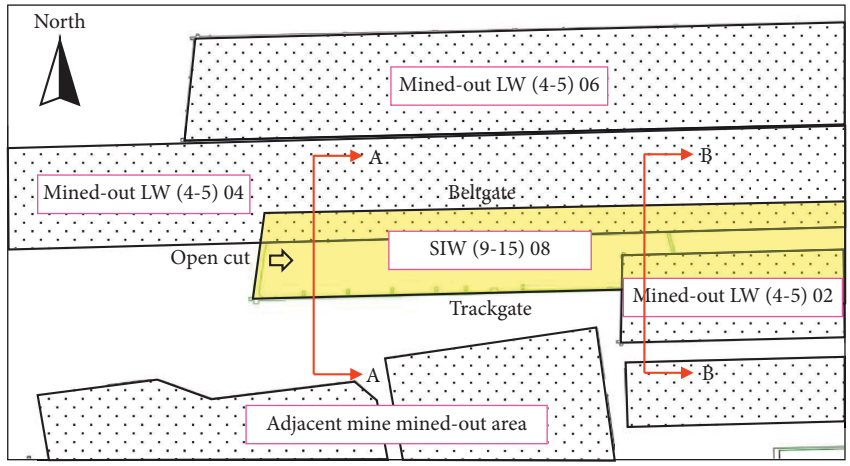

Figure 1: SIW(9–15) 08 plan location diagram.

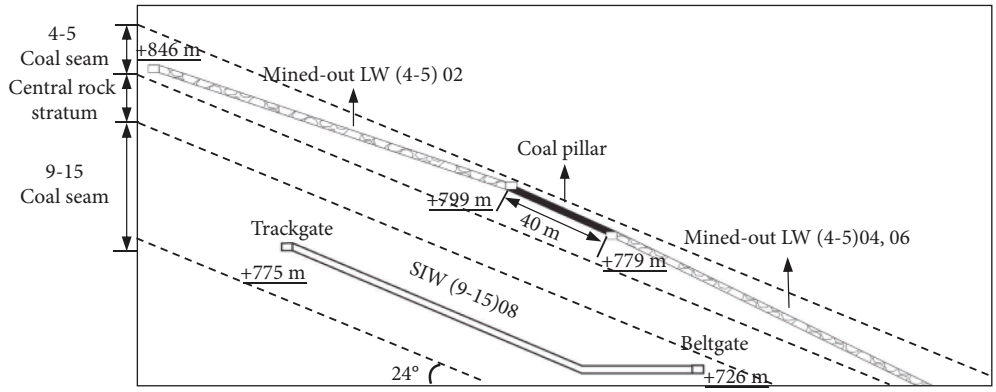

Figure 2: Schematic diagram of A–A tendency profile.

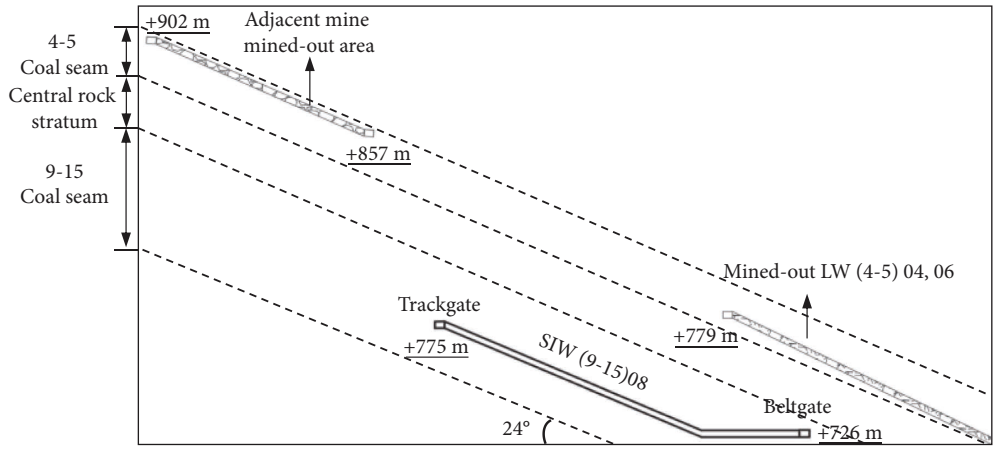

Figure 3: Schematic diagram of B–B tendency profile.

stress concentration of the coal body is much higher than that of the ordinary working face. But the coal body of the working face at this stage has a large bearing width, the peak stress distribution is not yet superimposed on both sides of the coal body, and the middle of the coal body is still in the original rock stress area, showing a "bimodal" distribution, as shown in Figure 5(a). There is no risk of overall instability rockburst in this stage.

At the middle stage of mining, as the working face continues to advance, the roof strata gradually break and are connected with the overlying faulted strata in the surrounding mined-out areas, forming a spatial structure similar to the "*C*" shape [30]. The stress peak gradually shifts to the middle of the coal body, and the stress in the center of the coal body rises above the original rock stress. At this point, the stress distribution is presented as a "saddle type," as shown in Figure 5(b).

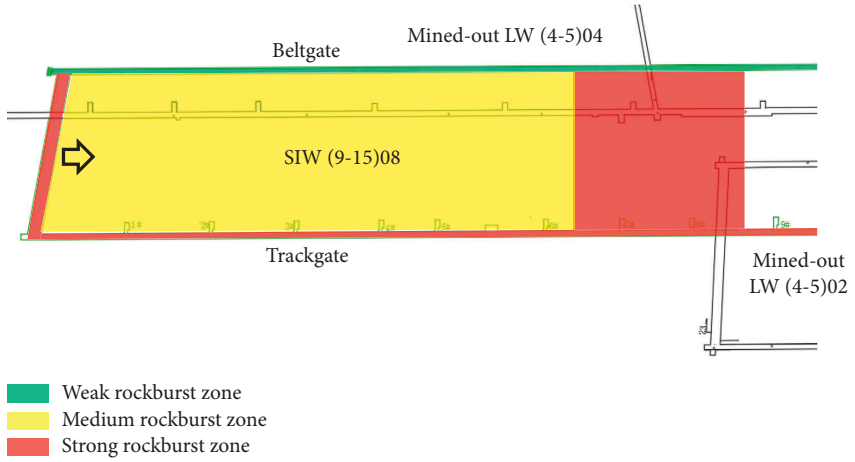

Figure 4: Rockburst danger zones of SIW(9–15) 08.

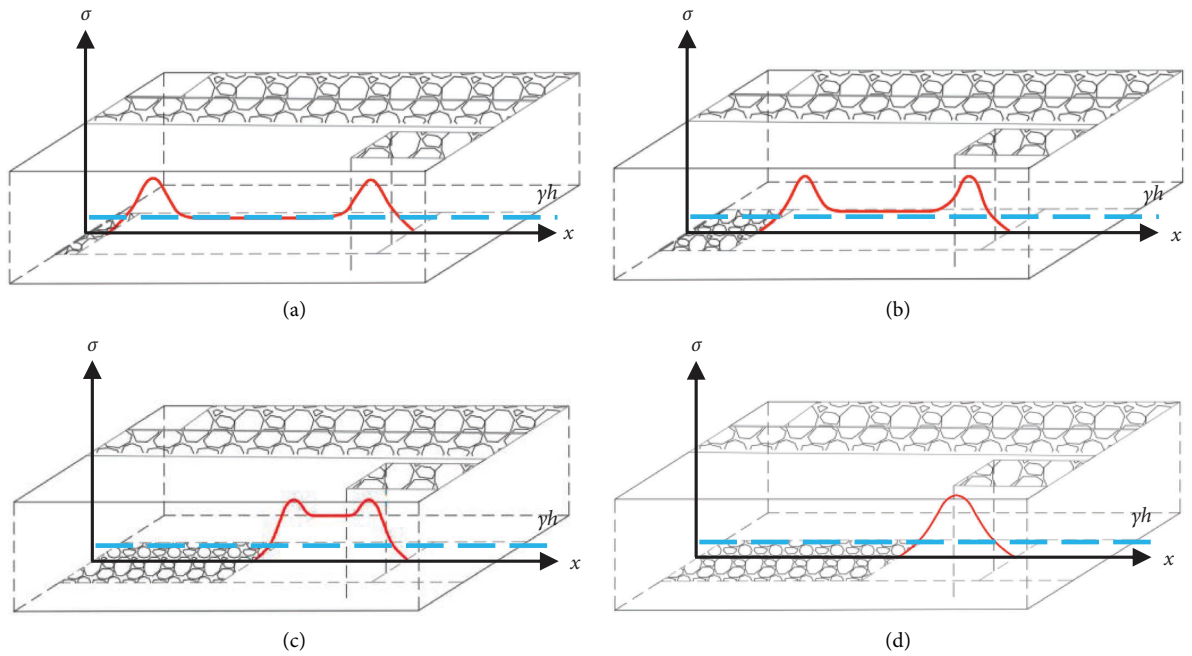

Figure 5: Schematic diagram of superimposed force field distribution. (a) Bimodal type. (b) Saddle type. (c) Platform type. (d) Unimodal type.

At the end stage of mining, the overburden spatial structure develops continuously upward, forming a dynamic "C" type overburden spatial structure. When the working face enters the influence range of side abutment pressure of mined-out LW(4-5) 02, the overlying strata on the working face gradually connect with the overlying broken strata of mined-out LW(4-5)02, forming a nearly "θ" type overlying rock spatial structure with coal body support in the middle [31]. At this time, the isolated coal body stress is "platform type" or even "unimodal type" distribution, as shown in Figures 5(c) and 5(d). The central region of the coal body stress increases sharply, the core stress homogenizes, and the overall instability rockburst is very easy to occur.

3.2. Mechanism and Mechanical Analysis. According to the previous analysis of the spatial structure and stress evolution of the overburden during the mining of (9–15) 08 working face, the mechanism of the overall instability rockburst of (9–15) 08 working face is: before working face mining, the coal body is not affected by mining disturbance, and the stress on the coal body mainly comes from the self-weight of the overlying strata and the transfer stress of the overlying strata on both sides of the mined-out areas and is in a state of stress equilibrium. During the working face mining, the isolated coal body will be affected not only by the above stresses, but also by the advanced support pressure of the working face, and gradually enter the side abutment pressure influence range of the mined-out LW(4-5)02, the advanced

support pressure of the working face and the side abutment pressure of the mined-out areas are superimposed, which further increases the risk of the overall instability rockburst of the coal body of the isolated working face.

In order to visually analyze the stresses on the coal body when the working face advances, the stresses on the isolated coal body are roughly divided into three parts: the working face inclined abutment pressure, the working face strike abutment pressure, and the self-weight of the overlying strata of the coal body.

3.2.1. Inclined Abutment Pressure Distribution Characteristics. According to the actual mining situation of the coal seam in the Liuhuanggou coal mine and the measured parameters of surface subsidence, it is known that the overlying strata of 4-5 coal seam are in a non-sufficient mining state after the working face of 4-5 coal seam had been mined. Since the 4-5 coal seam and 9–15 coal seam are only about 28 m apart, in order to simplify the calculation, it is assumed that (9–15) 08 working face is in the same plane as the mined-out areas on both sides. Accordingly, a static distribution model of the inclined abutment pressure of the coal body at the isolated working face is established, as shown in Figure 6.

The area S_1 of the red area on the left side is shown in

$$S_1 = \frac{l_1 \sin\theta}{2}\left(H_1 - \frac{l_1 \sin\theta}{2}\right)(1 + \cot\alpha_1) + \frac{l_1^2 \sin 2\theta}{16}(1 + \cot\alpha_1)^2 + \frac{\cot(\alpha_1 - \theta)}{2}\left(H_1 - \frac{l_1 \sin\theta}{2}\right)^2. \tag{1}$$

The area S_2 of the red area on the right side is shown in

$$S_2 = \frac{l_2 \sin\theta}{2}\left(H_2 - \frac{l_2 \sin\theta}{2}\right)(1 + \cot\alpha_2) + \frac{l_2^2 \sin 2\theta}{16}(1 + \cot\alpha_2)^2 + \frac{\cot(\alpha_2 - \theta)}{2}\left(H_2 - \frac{l_2 \sin\theta}{2}\right)^2. \tag{2}$$

The area S_3 of the yellow area on the left is shown in

$$S_3 = \frac{l_1^2}{16}(1 + \cot\alpha_1). \tag{3}$$

The area S_4 of the yellow area on the left is shown in

$$S_4 = \frac{l_2^2}{16}(1 + \cot\alpha_2). \tag{4}$$

Then, the average side abutment pressure on the isolated coal body is shown in

$$\overline{\sigma_l} = \sum_{i=1}^{4} S_i \frac{\gamma}{d}, \tag{5}$$

where l_1 and l_2 are the width of the mined-out areas on both sides of the isolated working face, H_1 and H_2 are the burial depth of the mined-out areas on both sides; d is the width of the isolated working face; α_1 and α_2 are the strata movement angles of the mined-out areas on both sides; θ is the dip angle of the coal seam; and γ is the volume weight of the overlying strata.

3.2.2. Strike Abutment Pressure Distribution Characteristics. The strike abutment pressure on the isolated working face is divided into two parts: mined-out LW(4-5) 02 strike abutment pressure and advanced support pressure when the working face advances. Taking the workface open cut as the coordinate origin and the direction of workface advance as the positive direction of the x-axis to establish the coordinate system, the incremental pressure of mined-out LW(4-5) 02 bearing pressure on the isolated work face is shown in

$$\Delta\sigma_3 = \begin{cases} 0, & \left[0, L - 2H_{i_3}\cot\beta_3\right], \\ 2\sigma_{\max i_3}\left[1 - \dfrac{(L-x)}{2H_{i_3}\cot\beta_3}\right], & \left[L - 2H_{i_3}\cot\beta_3, L - H_{i_3}\cot\beta_3\right], \\ \dfrac{\sigma_{\max i_3}(L-x)\tan\beta_3}{H_{i_3}}, & \left[L - H_{i_3}\cot\beta_3, L\right], \end{cases} \tag{6}$$

$$\sigma_{\max i} = \frac{(L_{wi} + H_i\cot\beta)M_i\gamma}{2H_i\cot\beta}, \tag{7}$$

where $\sigma_{\max i}$ is the maximum abutment pressure generated by the ith key stratum on the coal body on the side of the mined-out areas; H_i is the distance from the center of the thickness of the ith key stratum to the coal floor; β is the rock fracture angle in the mined-out areas; L_{wi} is the span of the key stratum i; and L is the length of the working face strike direction from the mined-out area.

The workface advanced abutment pressure stress increment $\Delta\sigma_4$ is shown in

$$\Delta\sigma_4 = \begin{cases} \dfrac{\sigma_{\max i}(x+a)\tan\beta}{H_{i_4}}, & \left[0, H_{i_4}\cot\beta\right], \\ 2\sigma_{\max i}\left[1 - \dfrac{(x+a)}{2H_{i_4}\cot\beta}\right], & \left[H_{i_4}\cot\beta, 2H_{i_4}\cot\beta\right], \\ 0, & \left[2H_{i_4}\cot\beta, L\right], \end{cases} \tag{8}$$

where a is the working face advance distance, taking the value range 0~L.

Combining equations (6)–(8), the strike average abutment pressure on the isolated coal body is shown in

$$\overline{\sigma_t} = \frac{\int_0^{L-a} \Delta\sigma_4 \mathrm{d}x + \int_a^L \Delta\sigma_3 \mathrm{d}x}{L - a}. \tag{9}$$

The self-weight stress of the coal body at the working face is shown in

$$\sigma_q = \gamma H, \tag{10}$$

where H is the depth of the working face.

Considering the effect of dynamic disturbance on the coal body of the isolated working face by mining activities

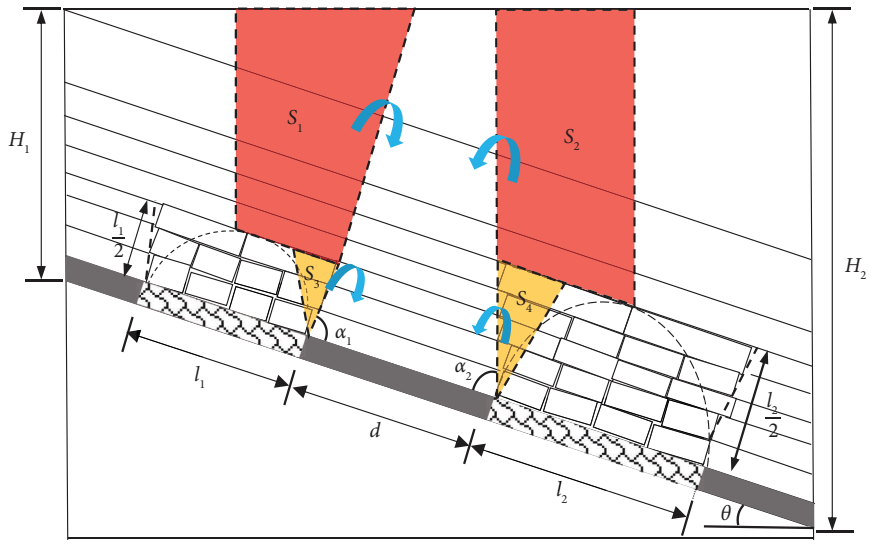

Figure 6: Static distribution model of inclined abutment pressure on the isolated working face.

[32, 33], introducing the dynamic load coefficient k, the average stress of the working face is shown in

$$\overline{\sigma} = k\left(\overline{\sigma_l} + \overline{\sigma_t} + \sigma_q\right). \tag{11}$$

3.3. Analysis of the Overall Instability Rockburst Hazard of a Spatially Isolated Working Face. The necessary condition for the occurrence of an overall instability rockburst on the coal body of an isolated working face is that the average abutment pressure on the isolated coal body exceeds 1.5 times its comprehensive compressive strength [34, 35]. We have the following equation:

$$I_c = \frac{\overline{\sigma}}{\overline{\mu}[\sigma_c]} > 1.5, \tag{12}$$

where $[\sigma_c]$ is the uniaxial compressive strength of the coal body, MPa, and $\overline{\mu}$ is the average comprehensive compressive coefficient of the coal body, taking the value range of 3~5.

It can be seen that when the average abutment pressure on the coal body of the isolated working face is equal to 1.5 times its comprehensive compressive strength, the isolated coal body is in the critical state of overall instability rockburst. Equation (13) can be obtained by associating equations (11) and (12):

$$k\left(\frac{\int_0^{L-a}\Delta\sigma_4 dx + \int_a^{L}\Delta\sigma_3 dx}{L-a} + \sum_{i=1}^{4} S_i\frac{\gamma}{d}\right) = 1.5\overline{\mu}[\sigma_c]. \tag{13}$$

Substitute the specific parameters of the working face into equation (13) and solve for the unknown a in the equation to obtain the limit advance distance of the working face when the isolated working face reaches the critical instability state.

3.4. Determination of the Overall Instability Rockburst Hazard

3.4.1. Estimation of Inclined Abutment Pressure. According to the relevant parameters of the adjacent mine and the working face of 04 and 06 of 4-5 coal seam, take the depth of the mined-out areas $H_1 = 350$ m, $H_2 = 486$ m; the width of the mined-out area $l_1 = 140$ m, $l_2 = 330$ m; the rock movement angle of the mined-out areas $\alpha_1 = \alpha_2 = 80^\circ$; (9–15) 08 working face width $d = 130$ m, coal seam dip angle $\theta = 24^\circ$, overlying strata volume weight $\gamma = 2.5$ t/m^3.

Substitute the above parameters into equations (1)–(5) to obtain the inclined abutment pressure as shown in

$$\overline{\sigma_l} = 29.85 \text{ MPa}. \tag{14}$$

3.4.2. Estimation of Strike Abutment Pressure. To simplify the calculation, the overlying strata of the mined-out areas are regarded as a whole rock formation, then $H_i = h_{\max} + M_i/2$. According to mined-out LW(4-5) 02 and SIW(9–15) 08 drilling stratigraphic parameters and field monitoring data, take mined-out LW(4-5) 02 depth $H_3 = 358$ m, pressure arch maximum height $h_{\max 3} = 70$ m, working face from the mined-out area strike length $L = 548$ m, (9–15) 08 working face buried depth $H_4 = 430$ m, $h_{\max 4} = 65$ m, $\beta_4 = 74^\circ$, key stratum span $L_{wi} = 417$ m.

Substituting the above parameters into equations (6)–(8) to obtain the strike abutment pressure and self-weight stress as shown in

$$\Delta\sigma_3 = \begin{cases} 0, & [0, 432], \\ 0.51x - 221.38, & [432, 490], \\ 280.54 - 0.51x, & [490, 548], \end{cases} \quad (15)$$

$$\Delta\sigma_4 = \begin{cases} 0.42\,(x + a), & [0, 69], \\ 64.04 - 0.42\,(x + a), & [69, 138], \\ 0, & [138, 548], \end{cases} \quad (16)$$

$$\sigma_q = 10.75. \quad (17)$$

3.4.3. Estimation of Limit Advance Distance. According to the identification data of coal seam 9–15 in the Liuhuanggou coal mine, the single axis compressive strength of coal body $[\sigma_c] = 21$ MPa, the average comprehensive compressive stress (CCS) coefficient of coal body $\mu = 3$, the dynamic load coefficient $k = 1.3$, and the comprehensive equations (14)~(17) can obtain the relationship between the average stress(AS) on the coal body of the isolated working face and the advancing degree of the working face as shown in Figure 7.

As can be seen from Figure 7, the AS on the coal body as the working face advances from the open cut to the mined-out LW(4-5) 02 is roughly divided into the following three stages:

(1) When the working face advances 350 m in the first stage, the AS of the coal body rises slowly with the advance of the working face, and the dynamic load stress of the working face increases slowly from 59 MPa to 76 MPa.

(2) When the working face advances 350~470 m and enters the influence range of mined-out LW(4-5) 02, the average stress on the coal body increases sharply, and the dynamic load stress on the working face increases rapidly from 76 MPa to 105 MPa. When the working face advances 430 m, the average stress on the coal body reaches the critical value of the overall instability rockburst, and the overall instability rockburst is very likely to occur.

(3) When the working face is pushed past the stress peak point of 470 m, the AS of the coal body decreases rapidly to below the critical value with the decrease of abutment pressure on the isolated coal body.

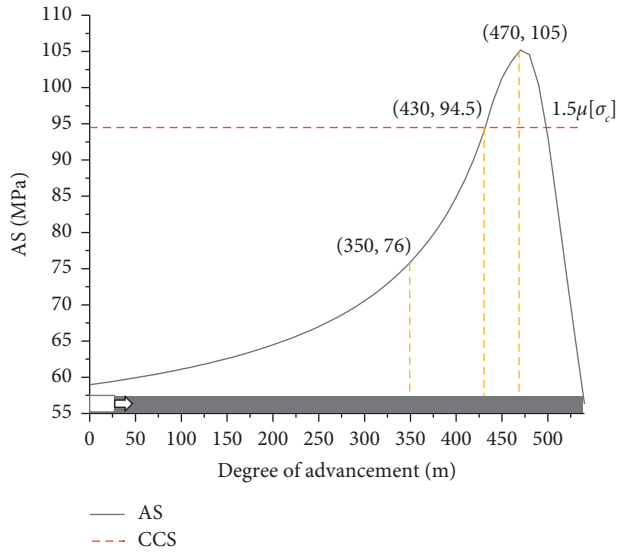

Figure 7: Relationship between average stress and degree of advancement of isolated coal body.

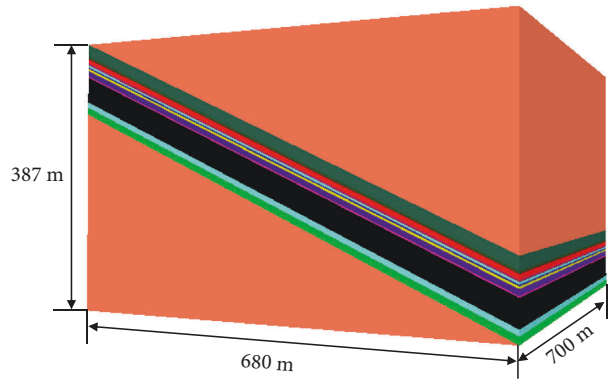

Figure 8: Numerical calculation model.

4. Numerical Analysis

4.1. Numerical Model. According to the geology and mining conditions of the Liuhuanggou coal mine (9–15) 08 working face, the model size is established as $L \times W \times H = 680\text{ m} \times 700\text{ m} \times 387\text{ m}$, with an inclination angle of 24°, using Mohr–Coulomb criterion, fixing the horizontal displacement at both ends of the model, constraining the horizontal and vertical displacement at its bottom, and the top as a free surface. Apply a uniform load on top of the model to simulate the self-weight of the overlying strata. Model X-axis direction is (9–15) 08 working face tendency, and Y-axis direction is (9–15) 08 working face direction. The numerical calculation model is shown in Figure 8.

4.2. Analysis of Stress Concentration. According to the actual mining situation of the adjacent mine and Liuhuanggou coal mine, the excavation sequence is adjacent mine working face ⟶ (4-5) 02 working face ⟶ (4-5) 04 working face-⟶ (4-5) 06 working face. The effect on the change of stress in the coal body of (9–15) 08 working face was recorded. The details are shown in Figure 9.

As can be seen from Figure 9, with the gradual hollowing around the (9–15) 08 working face, the stress on the coal body of the working face can be broadly divided into two areas:

(1) From Figures 9(a) and 9(c), it can be seen that when the adjacent mine working face is mined out, the working face coal body stress rises from 10.75 MPa to about 15 MPa. With the completion of mining of 04 and 06 working face of 4-5 coal seam, (9–15) 08

working face forms a spatial isolated working face with hollow mining on both sides, and the stress of coal body of working face rises obviously, from 15 MPa to about 40 MPa rapidly.

(2) From Figure 9(b), it can be seen that after (4-5) 02 working face is mined, the stress on the coal body of (9–15) 08 working face rises to about 17.5 MPa from the original rock stress by the influence of the mined-out area. When (9–15) 08 working face advances to the mined-out area, the abutment pressure transferred from the overlying strata of the mined-out area to the isolated coal body is gradually superimposed, and the stress on the coal body further increases. When the stress on the coal body exceeds its 1.5 times comprehensive compressive strength, there is a risk of overall instability rockburst.

4.3. Analysis of Stress Evolution during Mining. In order to study the stress changes of the isolated coal body at different advancement degrees of the working face, based on the results of the previous theoretical calculations, measurement lines were arranged along the middle of the inclination in the coal body of (9–15) 08 working face, focusing on monitoring the stress changes of the coal body when the working face is 200 m away from mined-out LW(4-5) 02, and recording the stress changes of the coal body at every 20 m advancement of the working face, as shown in Figure 10.

As can be seen from Figure 10, when the working face advances toward the mined-out LW(4-5) 02, the abutment pressure on the isolated coal body is distributed in a single peak, and the maximum point of the abutment pressure is about 100 m in front of the working face. When the working face advances in the range of 350~430 m, the abutment pressure on the isolated coal body increases continuously, and the peak stress increases from 55 MPa to 79 MPa, which increases the risk of overall instability rockburst on the coal body. After the working face advances 430 m, the stress decreases and tends to be stable. The abutment pressure drops back to about 53 MPa. From the numerical simulation analysis, it can be obtained that when the isolated working face gradually advances to about 430 m, the coal body abutment pressure gradually increases, and the risk of overall instability rockburst is higher.

5. Analysis of Safe Mining Plan and Effect

Based on the previous research on the overall instability mechanism of the isolated working face, the safe mining plan is designed from the perspective of monitoring and early warning, pressure relief for the actual situation of (9–15) 08 working face.

5.1. Monitoring and Early Warning Technical Measures. Monitoring and early warning technology are one of the most effective methods to prevent and control rockburst [36–41]. According to the previous analysis, "microseism-stress-drilling cutting" joint monitoring is carried out within 200 m from the front of mined-out LW(4-5) 02.

5.1.1. Microseismic Monitoring System Arrangement. Six microseismic probes are arranged within 200 m in front of the coal body of the working face and 100 m in the back mined-out area, among which three are arranged in the trackgate and beltgate respectively, using 100 m interval and cross arrangement to focus on monitoring the area with overall instability rockburst hazard. The microseismic probe arrangement is shown in Figure 11.

5.1.2. Online Stress Monitoring System Arrangement. During the mining of the working face, a measuring site is arranged every 25 m along the advancing direction, two measuring points are arranged in each site, and the installation depth of the borehole stress gauge is 14 m and 8 m, respectively, with an interval of 1 m. In the process of working forward to disassemble forward in time to ensure that the monitoring range is always not less than 200 m, as shown in Figure 12.

5.1.3. Arrangement of Drilling Cuttings Pulverized Coal Monitoring System. Pulverized coal monitoring is carried out within 60 m of the upper part of the beltgate and the lower part of the trackgate in the working face, with a hole depth of 15 m and a spacing of 20 m, and monitored twice a week. For the early warning areas monitored by the online stress monitoring system, one drilling cutting detection hole is constructed at a location 2~5 m from the early warning point, with the same drilling parameters as above.

5.2. Pressure Relief and Anti-Rockburst Technical Measures

5.2.1. Pre-Unloading Measures on Both Sides of the Working Face along the Gate. (9–15) 08 working face beltgate is located below the mined-out areas and has weak rockburst risk, so it is mainly monitored. If the rockburst hazard is found and then take pressure relief measures. (9–15) 08 working face trackgate is located in solid coal, with strong rockburst hazard, need to construct drilling relief with large diameter to unload pressure, drilling parameters as shown in Table 2.

5.2.2. Prepressure Relief Measures for Coal Wall at Working Face. According to the theoretical calculation and numerical simulation results, (9–15)08 working face will form a "θ" type overburden spatial structure when it is about 120 m away from mined-out LW(4-5) 02, which has the risk of overall instability rockburst, and it is necessary to take penetration pressure relief to eliminate the elastic core of coal column.

The original design was to take deep holes in the coal wall to relieve pressure after the working face entered the overall instability danger zone, due to the difficulty of the construction of this method, considering that (9–15) 08 working face needs to extract and release the gas in the coal body before mining, the research group proposed the "rockburst-gas" drilling technology, increasing the diameter of the gas extraction holes from 94 mm to 133 mm, with a spacing of 2 m and an

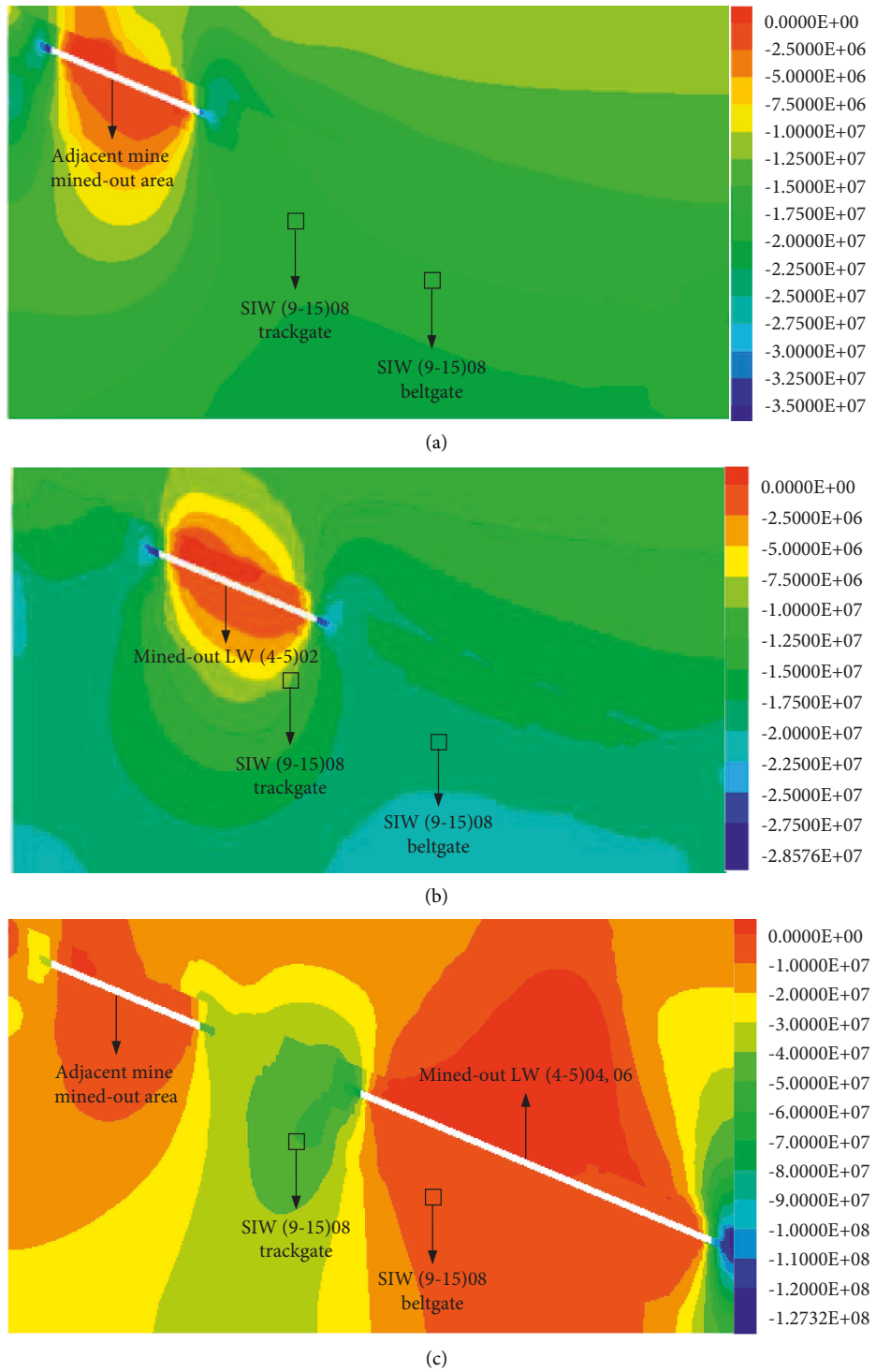

Figure 9: Stress evolution cloud diagram after mining at the working face. (a) Vertical stress cloud map of the adjacent mine working face after hollowing. (b) Vertical stress cloud map of the (4-5) 02 working face after hollowing. (c) Vertical stress cloud map of the (4-5) 04, 06 working face after hollowing.

inclination of 86°. The drill hole arrangement is shown in Figure 13.

During drilling construction, a large number of microseismic events were induced due to drilling activities. A comparison of microseismic events before and after the drilling construction is shown in Figure 14. Figure 14(a) shows the microseismic events during the normal mining period from July 6 to July 31 at (9–15) 08 working face, and

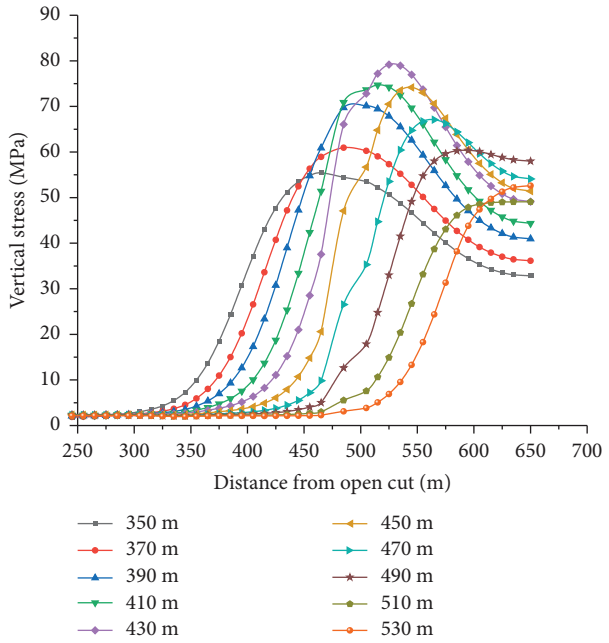

Figure 10: Stress changes of the isolated coal body.

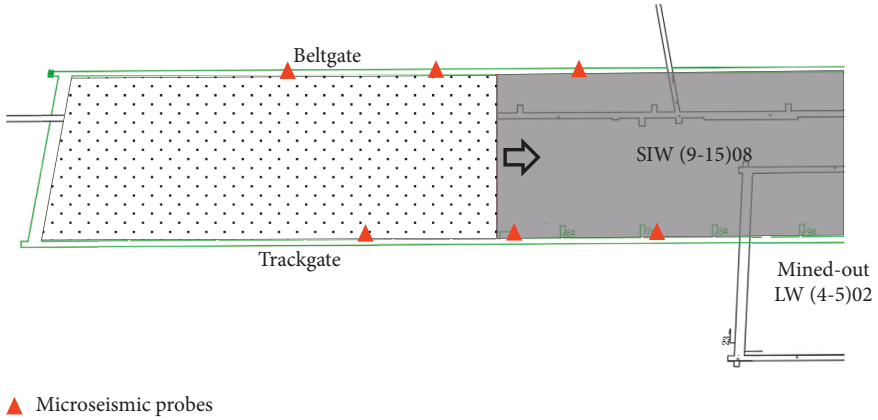

Figure 11: Schematic layout of the microseismic monitoring system.

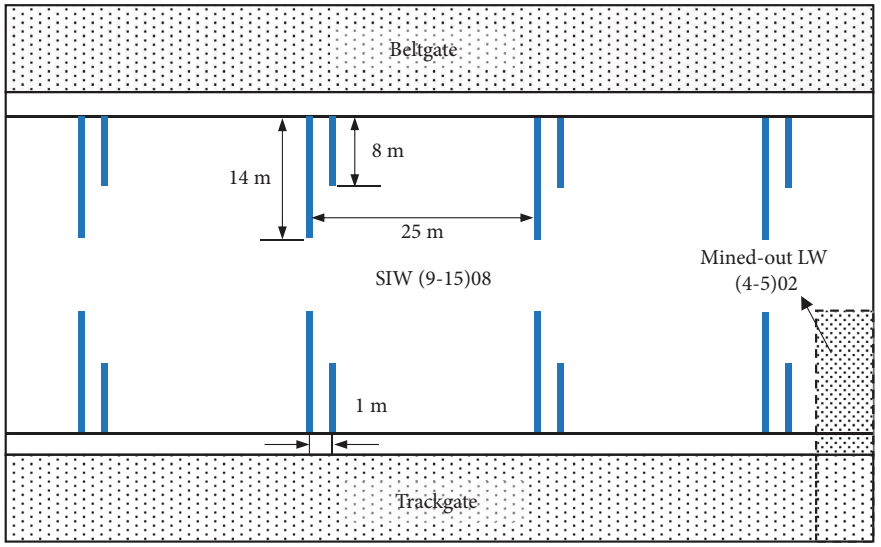

Figure 12: Schematic diagram of the measuring site layout.

Table 2: Prepressure relief measures and specific parameters of the two sides of the gate.

Rockburst hazard zone level	Measures	Parameters
Weak	Monitoring	—
Medium	Drilling relief with large diameter	Hole depth 25 m, drilling diameter 120~150 mm, hole spacing 2 m
Strong	Drilling relief with large diameter	Hole depth 25 m, drilling diameter 120~150 mm, hole spacing 1 m

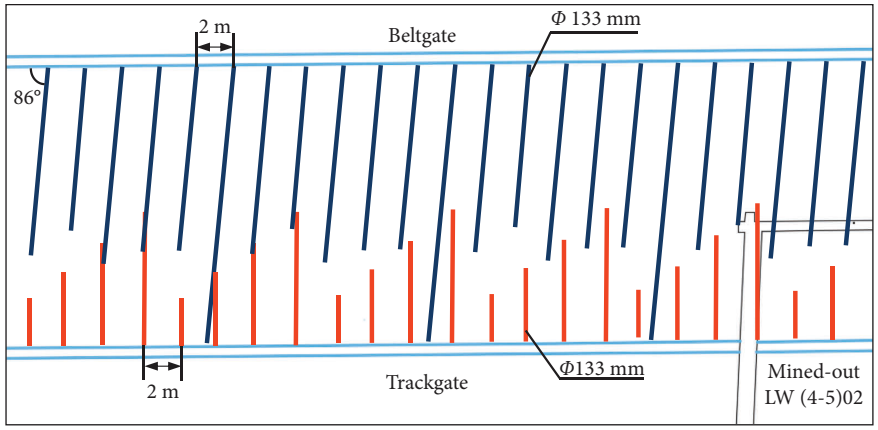

Figure 13: (9–15) 08 working face "rockburst-gas" drilling layout diagram.

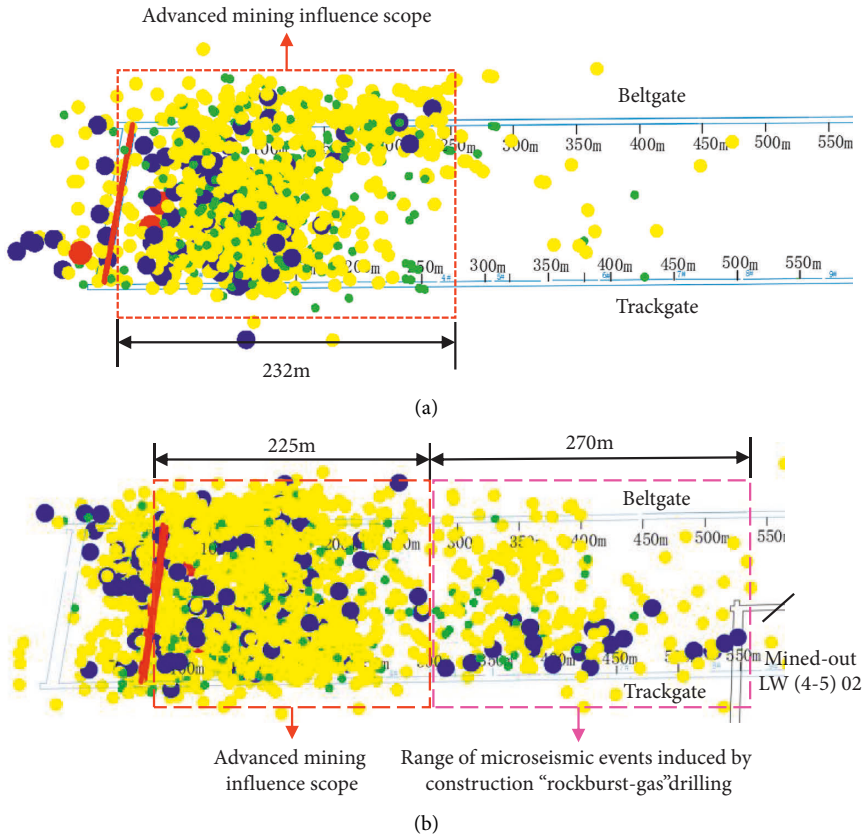

Figure 14: Comparison of microseismic events before and after the construction of "rockburst-gas" drilling. (a) Range of microseismic events during normal mining. (b) Range of microseismic events during drilling construction.

Figure 14(b) shows the microseismic events during the construction of the "rockburst-gas" drill hole at the coal wall of the isolated working face from August 28 to November 20. As can be seen from Figure 14, a large number of microseismic events occurred during the construction of "rockburst-gas" drilling in the overall instability rockburst hazard

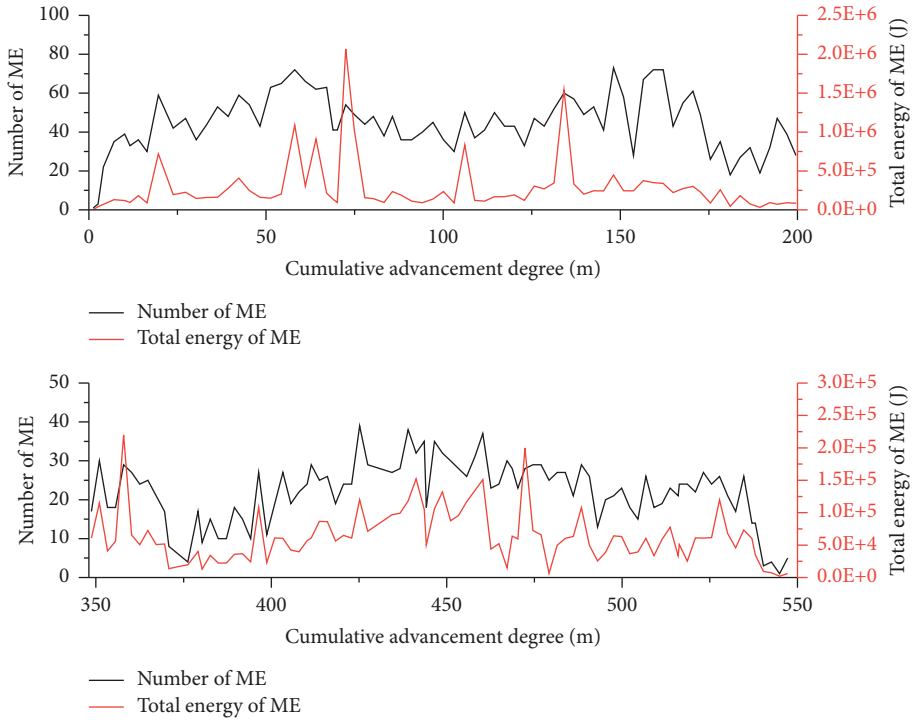

Figure 15: Comparison of microseismic events and total energy.

area of the working face, which released the elastic energy in the isolated coal body in advance and reduced the stress concentration in the coal column.

5.3. Control Mining Speed. Studies have shown that controlling the mining rate plays a crucial role in the prevention and control of rockburst [42, 43]. Excessive mining speed will lead to larger rock damage size, increased elastic energy released, abutment pressure peak in front of the coal body gradually approaching the coal wall, and the peak stress will increase.

According to the mining speed statistics of other working faces of 9–15 coal seam, the average mining speed of 9–15 coal seam is 2.8 m/d and the maximum mining speed is 5.6 m/d, which occurs in (9–15) 06 working face, during which no rockburst warning occurs. According to the results of theoretical calculation and numerical simulation, considering the high degree of stress concentration in the isolated coal body of (9–15) 08 working face and the risk of overall instability rockburst during the mining period, it is determined that the mining speed of the working face should not exceed 3.2 m/d when it is mining the fist 350 m of coal body, and the mining speed should not exceed 2.4 m/d when it enters the influence range of mined-out LW(4-5) 02 (350~550 m).

5.4. Strengthen the Strength and Distance of Advanced Support. From Figure 14, it can be seen that the advance disturbance range during the mining process of the working face is about 220 m, and the current advance support length of the mine is 120 m, so it is recommended to strengthen the

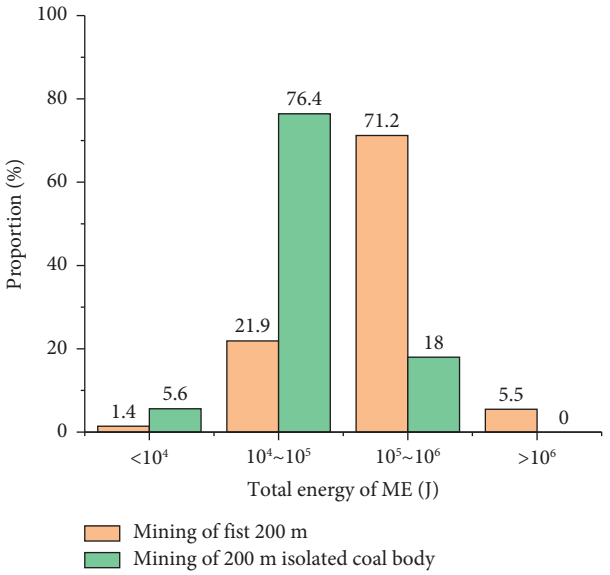

Figure 16: Total energy ratio of microseismic events.

advance support of the gateways of the working face to 220 m, and strengthen the strength of the advance support to improve the rockburst resistance and disturbance energy of the advance support system.

5.5. Analysis of Prevention and Treatment Effects. In order to test the prevention and control effect after taking targeted measures, the frequency and total energy of microseismic events (ME) occurring within 200 m of the initial advance of

the working face mining and 200 m of the advancement to the mined-out LW(4-5) 02 are compared, as shown in Figures 15 and 16.

From Figures 15 and 16, it can be seen that when the first 200 m of coal body was mined at the (9–15) 08 working face without special anti-rockburst measures, the highest number of microseismic events per day is 73. The total energy of microseismic events is up to 2.07×10^6 J, and 71.2% is concentrated in the range of 10^5~10^6 J. After taking special measures for safe mining, the number of daily microseismic events during mining of the isolated coal body decreased to 10~40, and the total daily microseismic energy is all less than 10^6 J, mostly located in the range of 10^4~10^5 J (76.4%). It can be seen that after the adoption of special measures for safe mining, the daily microseismic events and total energy decreased significantly compared with the initial stage of mining, which achieved the expected results and realized the safe mining of the overall instability rockburst hazard area of the isolated coal body.

6. Conclusion

Based on the Liuhuanggou coal mine (9–15) 08 spatially isolated working face as the engineering background, this article studies the stress evolution law of the isolated coal body, reveals the mechanism of its occurrence of overall instability rockburst of isolated coal, and pushes to the limit width when the coal body reaches the critical instability state. According to the actual mining situation of (9–15) 08 working face, this study proposes safety mining measures for isolated coal body. The effectiveness of the safety mining measures is verified by comparing the onsite microseismic monitoring data, and the following conclusions are drawn:

(1) Spatially isolated working face with increasing advance distance, the overlying strata show a dynamic transformation process from "*C*" type spatial structure to "*θ*" type spatial structure, and its susceptibility to overall instability rockburst is the result of the comprehensive effect of stress transfer from the working face and the overlying strata in the mined-out areas.

(2) According to the actual coal body storage condition, a mechanical analysis model is established to obtain the relationship between the internal stress of the coal body and the advancement degree, and the criterion for the limited advancement distance of the working face when the critical instability state is reached is derived. The results show that the working face reaches a critical instability state when it reaches 430 m from the open cut, and there is a risk of overall instability rockburst.

(3) Based on the results of the theoretical analysis, we have developed comprehensive prevention and control measures for monitoring and early warning, pressure relief and prevention, and control of mining speed, and proposed an innovative "rockburst-gas" drilling technology to ensure the safe mining of the isolated working face.

Data Availability

The data used to support the findings of this study are included within the article.

Conflicts of Interest

The authors declare no conflicts of interest.

Acknowledgments

This work was funded by the National Natural Science Youth Fund of China (51904017), China Association for Science and Technology Young Talent Support Project (2021QNRC001), and the Major Science and Technology Innovation Project in Shandong Province, China (2019SDZY02).

References

[1] H. Zhou, F. Meng, C. Zhang, D. Hu, F. Yang, and J. Lu, "Analysis of rockburst mechanisms induced by structural planes in deep tunnels," *Bulletin of Engineering Geology and the Environment*, vol. 74, no. 4, pp. 1435–1451, 2015.

[2] C. Zhang, I. Canbulat, B. Hebblewhite, and C. R. Ward, "Assessing coal burst phenomena in mining and insights into directions for future research," *International Journal of Coal Geology*, vol. 179, pp. 28–44, 2017.

[3] J. Zhou, X. Li, and H. S. Mitri, "Evaluation method of rockburst: state-of-the-art literature review," *Tunnelling and Underground Space Technology*, vol. 81, pp. 632–659, 2018.

[4] Z. Hao, G. Sun, and G. Zhang, "Mechanism and inducing factors of rockburst events of roadways under ultrathick strata," *Frontiers of Earth Science*, vol. 10, 2022.

[5] X. He, C. Zhou, D. Song et al., "Mechanism and monitoring and early warning technology for rockburst in coal mines," *International Journal of Minerals, Metallurgy and Materials*, vol. 28, no. 7, pp. 1097–1111, 2021.

[6] J. Zhang, F. Jiang, J. Yang, W. Bai, and L. Zhang, "Rockburst mechanism in soft coal seam within deep coal mines," *International Journal of Mining Science and Technology*, vol. 27, no. 3, pp. 551–556, 2017.

[7] L. Xu, K. Lu, Y. Pan, and Z. Qin, "Study on rock burst characteristics of coal mine roadway in China," *Energy Sources. Part A, Recovery, Utilization, and Environmental Effects*, vol. 44, no. 2, pp. 1–20, 2019.

[8] B. Liu, Y. Zhao, C. Zhang, J. Zhou, Y. Li, and Z. Sun, "Characteristic strength and acoustic emission properties of weakly cemented sandstone at different depths under uniaxial compression," *International Journal of Coal Science & Technology*, vol. 8, no. 6, pp. 1288–1301, 2021.

[9] Y. Jiang, Y. Zhao, H. Wang, and J. Zhu, "A review of mechanism and prevention technologies of coal bumps in China," *Journal of Rock Mechanics and Geotechnical Engineering*, vol. 9, no. 1, pp. 180–194, 2017.

[10] J. Zuo, H. Song, Y. Jiang, S. Zhao, M. Yu, and L. Li, "Preliminary discussion on comprehensive research method for rock burst in coal mine based on Newton's second law," *Shock and Vibration*, vol. 2020, Article ID 8861306, 16 pages, 2020.

[11] Q. X. Qi, Y. Z. Li, S. K. Zhao et al., "Seventy years development of coal mine rockburst in China: establishment and consideration of theory and technology system," *Coal Science and Technology*, vol. 47, no. 9, pp. 1–40, 2019, (in Chinese).

[12] Y. D. Jiang, Y. S. Pan, F. X. Jiang, L. M. Dou, and Y. Ju, "State of the art review on mechanism and prevention of coal bumps in China," *Journal of China Coal Society*, vol. 39, no. 2, pp. 205–213, 2014, (in Chinese).

[13] D. Guo, P. Lv, J. Zhao, and C. Zhang, "Research progress on permeability improvement mechanisms and technologies of coalbed deep-hole cumulative blasting," *International Journal of Coal Science & Technology*, vol. 7, no. 2, pp. 329–336, 2020.

[14] Q. Wang, S. Xu, M. He, B. Jiang, H. Wei, and Y. Wang, "Dynamic mechanical characteristics and application of constant resistance energy-absorbing supporting material," *International Journal of Mining Science and Technology*, vol. 32, no. 3, pp. 447–458, 2022.

[15] Q. Yin, J. Wu, Z. Jiang et al., "Investigating the effect of water quenching cycles on mechanical behaviors for granites after conventional triaxial compression," *Geomechanics and Geophysics for Geo-Energy and Geo-Resources*, vol. 8, no. 2, p. 77, 2022.

[16] P. Zhang, D. Zhang, Y. Yang et al., "A case study on integrated modeling of spatial information of a complex geological body," *Lithosphere*, vol. 2022, Article ID 2918401, 2022.

[17] Z. Dou, S. Tang, X. Zhang et al., "Influence of Shear Displacement on Fluid Flow and Solute Transport in a 3D Rough Fracture," *Lithosphere*, vol. 2021, no. 4, 2021.

[18] Z. Tao, Q. Geng, C. Zhu et al., "The mechanical mechanisms of large-scale toppling failure for counter-inclined rock slopes," *Journal of Geophysics and Engineering*, vol. 16, no. 3, pp. 541–558, 2019.

[19] M. Z. Gao, B. G. Yang, J. Xie et al., "The mechanism of microwave rock breaking and its potential application to rock-breaking technology in drilling," *Petroleum Science*, vol. 19, no. 3, pp. 1110–1124, 2022.

[20] C. Xue, A. Cao, W. Guo et al., "Mechanism and energy evolution characteristics of coal burst in mining thick, deep, and large inclined coal seams: a case study from a Chinese coal mine," *Geofluids*, vol. 2022, Article ID 7704226, 18 pages, 2022.

[21] S. Zhu, Y. Feng, and F. Jiang, "Determination of abutment pressure in coal mines with extremely thick alluvium stratum: a typical kind of rockburst mines in China," *Rock Mechanics and Rock Engineering*, vol. 49, no. 5, pp. 1943–1952, 2016.

[22] S. Zhu, Y. Feng, F. Jiang, and J. Liu, "Mechanism and risk assessment of overall-instability-induced rockbursts in deep island longwall panels," *International Journal of Rock Mechanics and Mining Sciences*, vol. 106, pp. 342–349, 2018.

[23] B. Wang, S. Zhu, F. Jiang, J. Liu, X. Shang, and X. Zhang, "Investigating the width of isolated coal pillars in deep hard-strata mines for prevention of mine seismicity and rockburst," *Energies*, vol. 13, no. 17, p. 4293, 2020.

[24] J. Deng and D. S. Gu, "Buckling mechanism of pillar rockbursts in underground hard rock mining," *Geomechanics and Geoengineering*, vol. 13, no. 3, pp. 168–183, 2018.

[25] G. Liu, Z. Mu, J. Chen, J. Yang, and J. Cao, "Rock burst risk in an island longwall coal face by stress field," *Geoscience Journal*, vol. 22, no. 4, pp. 609–622, 2018.

[26] Y. Xue, Z. Cao, and Z. Li, "Destabilization mechanism and energy evolution of coal pillar in rockburst disaster," *Arabian Journal of Geosciences*, vol. 13, no. 13, p. 557, 2020.

[27] T. Zhao, Y. Yin, F. Xiao, Y. Tan, and J. Zou, "Rockburst disaster prediction of isolated coal pillar by electromagnetic radiation based on frictional effect," *The Scientific World Journal*, vol. 2014, Article ID 814050, 7 pages, 2014.

[28] X. Shi, X. Zhang, and F. Jiang, "A case study of fracture law and stress distribution characteristics of surrounding rock of working face in deep mines," *Geotechnical & Geological Engineering*, vol. 37, no. 4, pp. 2935–2948, 2019.

[29] C. Wang, A. Cao, G. Zhu, G. Jing, J. Li, and T. Chen, "Mechanism of rock burst induced by fault slip in an island coal panel and hazard assessment using seismic tomography: a case study from Xuzhuang colliery, Xuzhou, China," *Geoscience Journal*, vol. 21, no. 3, pp. 469–481, 2017.

[30] J. B. Wang, M. D. Wang, E. X. Li, D. F. Dong, and L. M. Xu, "Advances and prospects of anginex as a promising anti-angiogenesis and anti-tumor agent," *Peptides*, vol. 38, no. 2, pp. 457–462, 2012.

[31] F. X. Jiang, "Viewpoint of spatial structures of overlying strata and its application in coal mine," *Journal of Mining & Safety Engineering*, no. 1, pp. 30–33, 2006, (in Chinese).

[32] K. Zhong, W. Zhao, C. Qin, H. Gao, and W. Chen, "Mechanical properties of roof rocks under superimposed static and dynamic loads with medium strain rates in coal mines," *Applied Sciences*, vol. 11, no. 19, p. 8973, 2021.

[33] Z. y. Wang, L. m. Dou, and G. f. Wang, "Mechanism analysis of roadway rockbursts induced by dynamic mining loading and its application," *Energies*, vol. 11, no. 9, p. 2313, 2018.

[34] F. X. Jiang, G. Cheng, Y. Feng, C. W. Wang, and Y. Y. Xu, "Research on coal overall instability of isolated working face with irregular gobs on both sides," *Chinese Journal of Rock Mechanics and Engineering*, vol. 34, no. S2, pp. 4164–4170, 2015, (in Chinese).

[35] G. A. Wang, S. T. Zhu, F. X. Jiang et al., "Mechanism of rock burst induced by overall instability of isolated coal and its prevention in large well at thousands-kilometer underground," *Journal of Mining & Safety Engineering*, vol. 36, no. 05, pp. 968–976, 2019, (in Chinese).

[36] X. l. Li, S. j. Chen, S. m. Liu, and Z. h. Li, "AE waveform characteristics of rock mass under uniaxial loading based on Hilbert-Huang transform," *Journal of Central South University*, vol. 28, no. 6, pp. 1843–1856, 2021.

[37] F. X. Jiang, S. H. Yang, Y. H. Cheng, X. M. Zhang, Z. Y. Mao, and F. J. Xu, "Astudyonmicroseismicmonitoringofrockburstincoalmine," *Chinese Journal of Geophysics*, vol. 49, no. 5, pp. 1511–1516, 2006.

[38] L. Qiu, Z. Liu, E. Wang, X. He, J. Feng, and B. Li, "Early-warning of rock burst in coal mine by low-frequency electromagnetic radiation," *Engineering Geology*, vol. 279, Article ID 105755, 2020.

[39] A. y. Cao, L. m. Dou, C. b. Wang, X. x. Yao, J. y. Dong, and Y. Gu, "Microseismic precursory characteristics of rock burst hazard in mining areas near a large residual coal pillar: a case study from xuzhuang coal mine, xuzhou, China," *Rock Mechanics and Rock Engineering*, vol. 49, no. 11, pp. 4407–4422, 2016.

[40] L. Qiu, Y. Zhu, D. Song et al., "Study on the nonlinear characteristics of EMR and AE during coal splitting tests," *Minerals*, vol. 12, no. 2, p. 108, 2022.

[41] Q. Wang, S. Xu, Z. Xin, M. He, H. Wei, and B. Jiang, "Mechanical properties and field application of constant resistance energy-absorbing anchor cable," *Tunnelling and Underground Space Technology*, vol. 125, Article ID 104526, 2022.

[42] H. Li, Q. Qi, W. Du, and X. Li, "A criterion of rockburst in coal mines considering the influence of working face mining velocity," *Geomechanics and Geophysics for Geo-Energy and Geo-Resources*, vol. 8, no. 1, p. 37, 2022.

[43] F. Cui, Y. Yang, X. Lai, C. Jia, and P. Shan, "Experimental study on the effect of advancing speed and stoping time on the energy release of overburden in an upward mining coal working face with a hard roof," *Sustainability*, vol. 12, no. 1, p. 37, 2019.